



Prestressed MF-FRP: Experimental Study of Rapid Retrofit Solution for Deteriorated Prestressed C-Channel Beams

Brad C. McCoy, Ph.D., P.E., M.ASCE¹; Zakariya Bourara²; Gregory W. Lucier, Ph.D.³; Rudolf Seracino, Ph.D., M.ASCE⁴; Min Liu, Ph.D., A.M.ASCE⁵; and Sheng-Hsuan Lin, S.M.ASCE⁶

Abstract: This paper presents design and installation details and full-scale test results for a prestressed mechanically fastened fiber-reinforced polymer (MF-FRP) retrofit solution that restores the original operating and inventory rating of prestressed concrete C-channel bridge superstructures with prestress losses due to concrete deterioration and steel corrosion. A retrofit solution that can be installed rapidly and immediately restores prestress losses is desired to minimize impacts on commerce, public transportation, and emergency services. Six 9.41-m (30-ft) long C-channel beams were tested for three-point bending to failure. The results of the experimental study indicate that the MF-FRP retrofit is capable of immediately restoring deteriorated C-channel beams with a 36% reduction in capacity from the original operating and inventory ratings. In this study, the reduction in the capacity of the C-channel beams was induced in the lab by cutting the bottom strand of each stem of the C-channel beam to simulate total prestress losses at the point of maximum internal moment. Further, the results of the experimental study indicate that the examined MF-FRP retrofit solution can be installed in 4.1 labor hours per retrofitted C-channel beam. Therefore, a four-worker DOT maintenance crew can install the retrofit on up to seven beams in a single eight-hour workday. A layered sectional analysis can be used to predict the flexural capacity of retrofitted C-channel beams with very good accuracy. **DOI: 10.1061/(ASCE) CF.1943-5509.0001536.** © 2020 American Society of Civil Engineers.

Author keywords: Strengthening and repair; Fiber-reinforced polymer (FRP); Mechanically fastened; Prestressed concrete; In-place concrete strength.

Introduction

Background

Prestressed concrete C-channel beams (hereafter referred to as C-channel beams) are among the common bridge superstructure elements in service across North Carolina and in many regions of the United States. North Carolina currently has 269 bridges across the state with prestressed concrete C-channel superstructures, of which 226 have load restrictions posted (or are closed) due to superstructure deterioration (North Carolina DOT 2018).

¹Assistant Professor, Dept. of Civil and Mechanical Engineering, United States Military Academy, West Point, NY 10996 (corresponding author). ORCID: https://orcid.org/0000-0003-0082-8214. Email: brad.mccoy@westpoint.edu

²Formerly, M.S. Graduate Student, Dept. of Civil, Construction, and Environmental Engineering, North Carolina State Univ., Raleigh, NC 27695. Email: zbourar@ncsu.edu

³Associate Research Professor, Dept. of Civil, Construction, and Environmental Engineering, North Carolina State Univ., Raleigh, NC 27695. ORCID: https://orcid.org/0000-0002-6648-9596. Email: gwlucier@ncsu.edu

⁴Professor, Dept. of Civil, Construction, and Environmental Engineering, North Carolina State Univ., Raleigh, NC 27695. Email: rseraci@ncsu.edu

⁵Associate Professor, Dept. of Civil, Construction, and Environmental Engineering, North Carolina State Univ., Raleigh, NC 27695. Email: mliu2@ncsu.edu

⁶Ph.D. Candidate, Dept. of Civil, Construction, and Environmental Engineering, North Carolina State Univ., Raleigh, NC 27695. Email: slin22@ncsu.edu

Note. This manuscript was submitted on February 25, 2019; approved on July 17, 2020; published online on October 23, 2020. Discussion period open until March 23, 2021; separate discussions must be submitted for individual papers. This paper is part of the *Journal of Performance of Constructed Facilities*, © ASCE, ISSN 0887-3828.

Deterioration of the C-channel beams often results in prestress losses and requires both inventory and operating rating levels to be reduced to satisfy AASHTO requirements (AASHTO 2018). These reduced operating and inventory ratings, commonly referred to as load restrictions, are categorized by AASHTO (2018) as (1) single vehicle (SV); and (2) truck tractor semitrailer (TTST). Table 1 provides a summary of the in-service C-channel bridges across North Carolina. An example of a deteriorated prestressed C-channel beam bridge is provided in Fig. 1. The deterioration in Fig. 1(b) is due to agricultural run-off; however, similar deterioration occurs in chloride environments along the coast, resulting in prestress losses from concrete spalling and steel corrosion.

The 226 restricted or closed bridges across North Carolina have an average detour length of 12.6 and 12.1 km (7.8 and 7.5 mi) for SV and TTST vehicles, respectively. These detours increase vehicle operating costs (VOC) for industries that routinely use routes with restricted bridges. Although not the focus of this paper, a previous North Carolina DOT study concluded that the average VOC for vehicles greater than 231 kN (26 t) is \$1.61/km (\$2.59/mi), and it is \$1.16/km (\$1.86/mi) for vehicles less than 231 kN (26 t) (Cavalline et al. 2015). The results of Cavalline et al. (2015) indicate that the detours for the previously discussed 226 load restricted bridges directly cost each detoured vehicle owner approximately \$14–\$20 each way. Further, the study concluded that the average detour speed is 64.5 km/h (40 mph), resulting in an 11.7-min average detour time for SV vehicles and an 11.3-min average detour time for TTST vehicles.

The detours due to bridge load restrictions and closures affect industry and public transportation and emergency services. Table 2 provides the number of C-channel bridges in North Carolina with restrictions that detour a typical type C school bus (151 kN/16 t), a typical pumper truck fire apparatus (187 kN/21 t), and a typical aerial ladder truck fire apparatus (338 kN/38 t) (FAMA 2017). Using an average emergency vehicle travel speed of 72.5 km/h

(45 mph) increases the response times for pumper trucks and aerial ladder trucks by approximately 9 and 12 min, respectively (Table 2). These increases alone are more than double the US national benchmark response time of 5 min (Ammons 2001). Additionally, North Carolina is one of 21 states in the United States that do not exempt emergency service vehicles from bridge load restrictions (FAMA 2017). Therefore, it is reasonable to include load restriction detours in emergency service response times in North Carolina and all non-exempt states.

AASHTO Bridge Rating Requirements

AASHTO (2018) requires bridges to be rated for the two categories of operating and inventory rating. McCoy (2019) described in detail the requirements for each rating criteria. A summary is provided to sufficiently inform the reader of the rating requirements and criteria that must be addressed to remove or reduce load restrictions on deteriorated prestressed concrete bridges.

Inventory rating criteria address routine traffic and establish the maximum vehicle load that can be applied to the bridge without damage for an indefinite period and an indefinite number of cycles. Inventory ratings are typically based on serviceability stress limits and reflect the existing bridge condition as determined through routine bridge inspection processes. In prestressed concrete bridge superstructures, concrete tensile stresses typically control the inventory rating. Operating rating criteria address nonroutine traffic and establish a maximum vehicle load that typically exceeds the inventory rating stress limit; therefore, incremental damage may occur at this load limit. The operating rating is based on strength limit states and is typically a specified factor of the ultimate strength capacity. In most cases, the operating rating controls bridge capacity

Table 1. North Carolina C-channel bridge restriction summary

	SV	TTST
Total posted restrictions	225	208
Percent posted (%)	83.6	77.3
Average restriction value (kN/t)	227/25.5	267/30.0
Median restriction value (kN/t)	214/24	258/29
Minimum restriction (kN/t)	44.5/5	44.5/5
Maximum restriction (kN/t)	365/41	400/45
Total closures	1	3
Average detour (km/mi)	12.6/7.8	12.1/7.5

and load restrictions. However, in deteriorated prestressed concrete bridge superstructures in which prestress losses allow inventory vehicle loading to develop tensile stresses in the concrete, both the inventory and operating rating criteria must be addressed to adequately remove posted load restrictions.

A feasible retrofit solution must restore prestress losses such that concrete stress limits at service load levels are within AASHTO (2018) allowable limits

$$f_{t,allow} = 0.5\sqrt{f_c'} \text{ (MPa)}$$
 (1a)

or

$$f_{t,allow} = 6\sqrt{f_c'} \text{ (psi)}$$
 (1b)

where $f_{t,allow}$ = allowable concrete tensile stress; and f_c' = concrete design compressive strength. Eq. (1) represents the controlling inventory rating criteria for prestressed C-channel beams (McCoy 2019). Additionally, many bridge owners, in accordance with AASHTO (2018) provisions, further reduce $f_{t,allow}$ to $0.25\sqrt{f_c'}$ (MPa) or $3\sqrt{f_c'}$ (psi), or 0 depending on environmental conditions. Therefore, to address the most conservative tensile stress limits, a desirable retrofit solution must be capable of limiting the concrete tensile stress to zero at inventory rating levels and must be capable of restoring the ultimate strength capacity such that the operating rating of a deteriorated C-channel beam is equal to or greater than the original operating rating.

Existing Retrofit Solutions

Externally prestressed steel strands have been used to retrofit reinforced concrete structures that require strengthening (Tan and

Table 2. Total C-channel bridge restrictions impacting public service vehicles

Vehicle type	SV	TTST	Average detour length (km/mi)	Average detour time (min)
Type C school bus Pumper truck fire apparatus Aerial ladder truck fire apparatus	13	N/A	24/15	22.5
	68	N/A	11/6.8	9.1
	N/A	177	14/8.7	11.6





Fig. 1. Example C-channel deterioration: (a) wide view of C-channel bridge; and (b) underside of deteriorated C-channel. (Images by Rudolf Seracino.)

Tjandra 2007) and could feasibly be used to restore prestress losses in deteriorated prestressed concrete structures. However, because many deteriorated prestressed concrete bridges require repair due to corrosion of the internal steel, the external steel strands are likely to be even more susceptible to corrosion when exposed to aggressive environments. Further, the installation of externally prestressed strands is labor intensive and requires the use of hydraulic equipment to apply the jacking force.

Because of its inherent resistance against corrosion, FRP is desirable material for the repair of bridge superstructures. The current state-of-practice for the repair of deteriorated concrete bridge superstructures using FRP includes externally bonded (EB), mechanically fastened (MF), and a combination of both (hybrid). EB-FRP systems present challenges in verification of the bond quality at the time of installation and during subsequent inspections (Oehlers and Bradford 1995). EB systems also require increased installation time due to bond curing requirements and can suffer premature brittle failure due to mechanical debonding or chemical deterioration of the adhesive (Oehlers and Bradford 1995). Although it is possible to prestress EB-FRP systems (Piatek et al. 2020), the quality of the adhesive bond remains critical, and adequate surface preparation of the concrete substrate is required. The installation process is time and labor intensive and requires specialized equipment. Because of these characteristics, an EB-FRP solution is not considered desirable and, thus, is not the subject of this research.

MF-FRP strengthening solutions are the subject of previous research largely focused on fastener type and concrete-fastener interaction. This previous research is presented in detail by McCoy et al. (2019) and summarized in Table 3. This existing study serves as the

basis for the development of the bolt pattern used in the proposed retrofit solution. Bank et al. (2002) presented two projects that examine increased operating ratings for reinforced concrete bridge decks using MF-FRP. The use of MF systems addresses many of the concerns associated with EB systems, and prestressing MF-FRP can be used to address the inventory rating shortcoming. Additionally, Knight et al. (2014) presented a mechanics-based, partial-interaction, moment-rotation approach to predict the response of MF-FRP-strengthened reinforced concrete beams. Lastly, because freeze-thaw cycling and saltwater intrusion are of concern with many deteriorated bridges in cold weather climates and coastal regions, Loring and Davids (2015) demonstrated that hybrid glass-carbon MF-FRP flexural strengthening systems exhibit sufficient resistance to the deleterious effects of these environmental conditions.

McCoy (2019) presented an extensive review of the current state-of-the-art and state-of-practice to strengthen and repair concrete bridge superstructures using FRP. The current body of knowledge does not include a rapid installation of a prestressed solution using EB-, MF-, or hybrid-FRP approaches that restores prestress losses due to the deterioration of prestressed concrete bridge superstructures.

The 226 C-channel bridge restrictions and closures across North Carolina increase travel time and VOC and decrease emergency response capabilities, significantly impacting commerce and residents' lives. Current solutions available to address the deterioration of prestressed concrete bridge superstructures are limited to the following: (1) immediate superstructure replacement; (2) temporary posted restrictions or closures until superstructure replacement can be scheduled; or (3) long-term restrictions or closures. In most cases in North Carolina, the scheduling process for bridge

Table 3. MF-FRP literature summary

		Faster	ner		_
Source	Туре	d_f (mm)	l_f (mm)	No. lines ^a	Test type
Borowicz (2002)	PAF ³	4.45	47.0	2-a	
Ebead (2011)	Screw	4.75	38.1	1-a/2-a	
Ekenel et al. (2006)	Wedge	9.53	40.6	1-s	
El-Maaddawy (2014)	PAF	3.99	32.0	2-a	
	Wedge	8.00	55.1	1-s	
	Screw	8.00	55.1	1-s	
El-Maaddawy et al. (2013)	DAE3	2.00	32.0	1-a/2-a	
•	PAF^3	3.99	52.1	1-a/2-a	
Galati et al. (2007)	Wedge	12.0	99.8	1-s/2-a	
Lamanna (2002)		3.99	22.0	2-a	
	PAF^3	3.71	26.9	1-a	4D D 1'
		3.71	32.0	1-a	4P Bending
Lamanna et al. (2001)	DAE3	3.48	26.9	2-a	
	PAF^3	3.71	32.0	1-a	
Bank et al. (2002)	PAF^3	4.50	32.0	2-a	
Lamanna et al. (2004)	PAF^3	4.50	47.0	2-a	
Lee et al. (2009)	DAE3	3.48	25.0	2-a	
	PAF^3	3.48	32.0	2-a	
Bank and Arora (2007)	PAF ³ /Wedge	4.07/12.7	44.5/69.9	1-a	
Martin and Lamanna (2008)	Screw	12.7	50.8	1-a/1-s	
Napoli et al. (2013)	Screw	9.53	44.5	1-s	
Dempsey and Scott (2006) ^b	Screw	4.50	50.8	2-a	
Realfonzo et al. (2013)	G	7.00		1-a	
,	Screw	5.99	45.0	2-s	Tension
Elsayed et al. (2009)	PAF^3	3.73	47.0	1-a	Telision
Elsayed et al. (2009)	Screw	4.75	36.8	1-a/2-a	

Source: Reprinted from McCoy et al. (2019), ©ASCE.

Note: a = aligned lines; s = staggered lines; and PAF = powder actuated fastener.

^aLines are in the longitudinal direction.

^bMF-FRP applied to timber elements.

replacement takes three to five years, including the time required for capital project funding and the design-bid-build or design-build project delivery cycles. Therefore, an acceptable retrofit solution must restore prestress losses due to deterioration for a period of three to five years. Additionally, it is desired that the solution be installed rapidly and be easily inspected and maintained. Such a system would allow deteriorated C-channel beams to remain in service without posted load restrictions or closures when a permanent superstructure replacement is scheduled and completed.

Research Significance

This paper presents a proof-of-concept for two MF-FRP retrofit solution designs and describes the behavior of the MF-FRP retrofit solutions employed on previously in-service, full-scale C-channel beams tested for failure in flexure. The behavior of beams strengthened with the proposed MF-FRP retrofit are presented for damaged (deteriorated) and undamaged C-channel sections and are useful for the ongoing development of a field-ready MF-FRP retrofit solution for DOTs to address prestress loss in deteriorated C-channel beams. Additionally, the results of the full-scale tests presented here can be used to develop other MF-FRP retrofit solutions that restore minor to moderate prestress losses in deteriorated superstructure elements across a range of cross-sections. The MF-FRP retrofit solution examined in this study was post-tensioned to restore prestress losses and satisfy both inventory and operating rating requirements.

MF-FRP Retrofit Design

MF-FRP 1.0

McCoy et al. (2019) presented a 22-bolt anchor pattern, indicated in Figs. 2(c and d), using 12.7-mm (0.5-in.) diameter bolts arranged in two aligned 11-bolt rows with 38-mm (1.5-in.) transverse spacing between rows. This pattern was proven sufficient to develop approximately 90% of the full capacity of the FRP plate with holes and is sufficiently optimized with respect to the number of bolts and peak bearing stresses in the FRP plate. The capacity of the 22-bolt anchor pattern presented by McCoy et al. (2019) is 200 kN (45 kips).

The initial MF-FRP retrofit design (MF-FRP 1.0) indicated in Figs. 2 and 3 incorporates the 22-bolt anchor pattern by attaching the FRP plate directly to the concrete on the interior of each Cchannel stem at one end (dead-end) [Figs. 2(a and c) and 3(a)]. The MF-FRP retrofit was attached to the interior only because adjacent beams in the field prevent access to the stem exteriors. The FRP plate was attached to a steel connector plate at the opposite end (liveend) [Figs. 2(d) and 3(b)] using the same 22-bolt anchor pattern. The steel connector plate at the live-end was joined to a steel fixed plate through a welded coupler and turnbuckle system [Fig. 2(b)], and the fixed plate was connected to the interior of the C-channel stem through six 18.8-mm (0.75-in.) diameter bolts [Fig. 2(b)]. All components of the MF-FRP 1.0 connection were designed in accordance with AISC design guidelines (AISC 2015) such that the design strength exceeds the 200-kN (45-kip) capacity of the 22-bolt FRP connection. Hence, the connection between the FRP plate and steel connector plate is the controlling design element.

MF-FRP 1.0 required 28 holes drilled per stem for the 22-bolt FRP connection at the dead-end, and the six-bolt steel connection at the live-end. A pachometer was used to locate the high-strength (HS) strands and shear reinforcement prior to drilling, and the placement of the MF-FRP system was adjusted to avoid the HS strands and shear reinforcement in the C-channel stems. All holes were drilled

using a commercially available hammer drill. A portable dust collection system with a snorkel attachment in accordance with Occupational Safety and Health Administration (OSHA 2018) requirements was used to mitigate the effects of respirable crystalline silica dust during drilling operations. Although care was taken to minimize spalling due to drilling, moderate concrete spalling occurred at each hole during drilling. This spalling was repaired at the dead-end with high-strength grout to create a flat surface for the 22-bolt FRP-to-concrete connection [Fig. 3(a)]. At the live-end, the spalling was not repaired because it was determined that sufficient concrete remained at each hole to give the required bearing surface area at each bolt, and the spalled surface did not impact the installation of the steel base plate. All bolts in steel-to-concrete bolted connections extended through the entire stem thickness. Wedge washers were used to provide even force distribution against the tapered side of the C-channel stems [Figs. 2(a and b)].

MF-FRP 2.0

The performance of MF-FRP 1.0 presented the following two critical observations, which are subsequently discussed in greater detail: (1) drilling 28 holes in each stem of the C-channel beam was time and labor intensive, and (2) the 22-bolt dead-end connection created a fixity that resulted in an in-plane moment about the strong-axis of the FRP plate as the beam deflected. This developed transverse stresses in the FRP plate along the bolted connection and reduced the capacity of the MF-FRP system. Therefore, a second MF-FRP retrofit design (MF-FRP 2.0) was developed to reduce field drilling requirements and to allow the FRP plate to remain in uniaxial tension throughout the test. Holes were drilled using the procedures described previously. Details of MF-FRP 2.0 are presented in Figs. 4 and 5.

MF-FRP 2.0 used a fixed plate connection at each end of the C-channel beam to transfer the forces between the MF-FRP system and the beam. Forces were transferred through six 18.8-mm (0.75-in.) diameter bolts at each end of the C-channel beam (Figs. 4 and 5), similar to the live-end of MF-FRP 1.0. The transverse spacing between the fixed plate bolts was reduced to 76.2 mm (3.0 in.) (Fig. 4) to optimize the design with respect to concrete splitting behavior and to reduce the weight of the 50-mm (2-in.) fixed plate such that one worker can lift the plate into place during installation. The fixed plate was connected to an FRP connector plate at the dead-end [Fig. 5(a)] and a turnbuckle (TB) connector plate at the live-end [Fig. 5(b)] through a pin connection to allow rotation and prevent internal moment in the FRP plate as the beam deflected under applied loads. The TB connector plate connected to the turnbuckle and FRP connector plates at the live-end through a welded connection [Figs. 4(b) and 5(b)] configured such that the centerline of the turnbuckle and connector plates were aligned to minimize internal moment due to eccentricity. Additionally, the effective depth of the FRP centroid from the top compression surface of the C-channel was 272 mm (11 in.) in MF-FRP 1.0 [Figs. 2(a and b)] and 330 mm (13 in.) in MF-FRP 2.0 [Fig. 4(a)]. This 18% increase in effective depth increased the effectiveness of the FRP, reducing the FRP tensile force required for the same level of strengthening compared with MF-FRP 1.0.

MF-FRP 2.0 was optimized in accordance with AISC (2015) design guidelines with a design strength of 222 kN (50 kips) for the steel connection components—11% greater than the ultimate strength of the FRP plate in uniaxial tension. Therefore, similar to MF-FRP 1.0, the controlling limit state of MF-FRP 2.0 is the connection between the FRP plate and the steel connector plate.

Factors other than design strength influence the thickness of the fixed plate in both connection designs. The thickness of the fixed

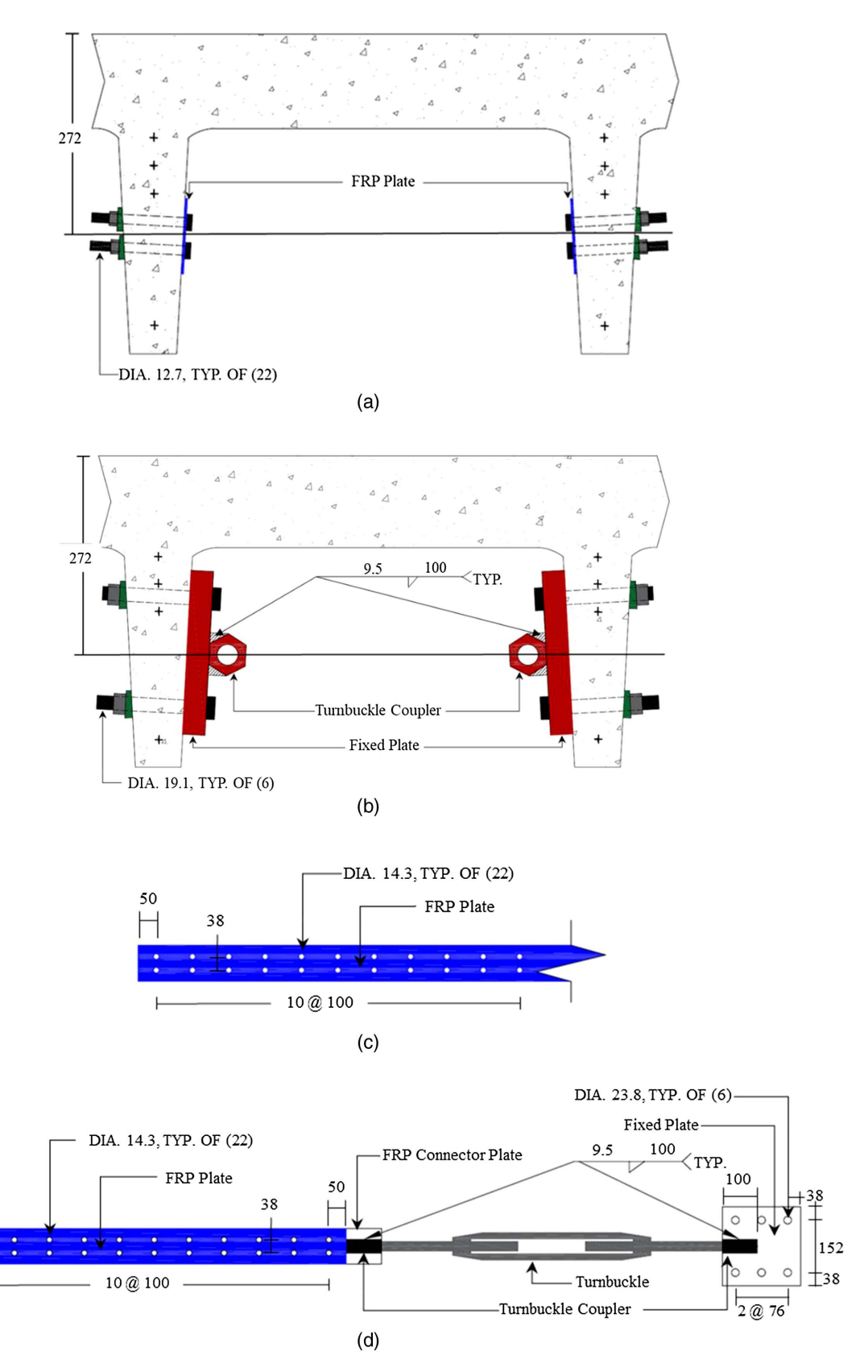


Fig. 2. MF-FRP 1.0 design details: (a) dead-end cross-section detail; (b) live-end cross section detail; (c) dead-end elevation detail; and (d) live-end elevation detail.

plate for MF-FRP 1.0 was 32 mm (1.25 in.) to provide clearance between the concrete stem and turnbuckle such that the body of the turnbuckle could be rotated. The thickness of the fixed plate for MF-FRP 2.0 was controlled by the shoulder length (38 mm/1.5 in.)

and head thickness (25 mm/1.0 in.) of the commercially available shoulder bolt that was used as the pin connection in Figs. 4 and 5. A custom turnbuckle or pin connection could be designed to further reduce the thickness of the fixed plate.

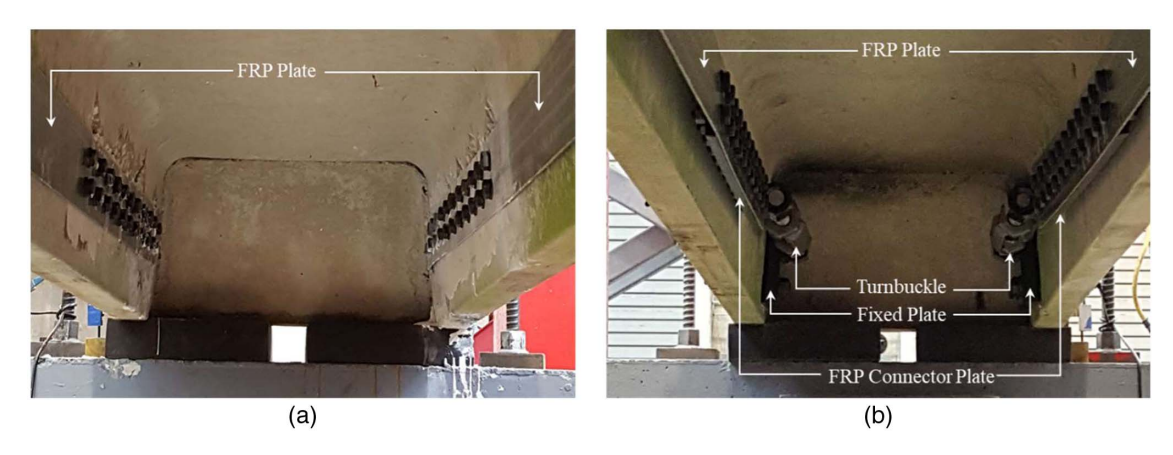


Fig. 3. MF-FRP 1.0 connection photos: (a): dead-end; and (b) live-end.

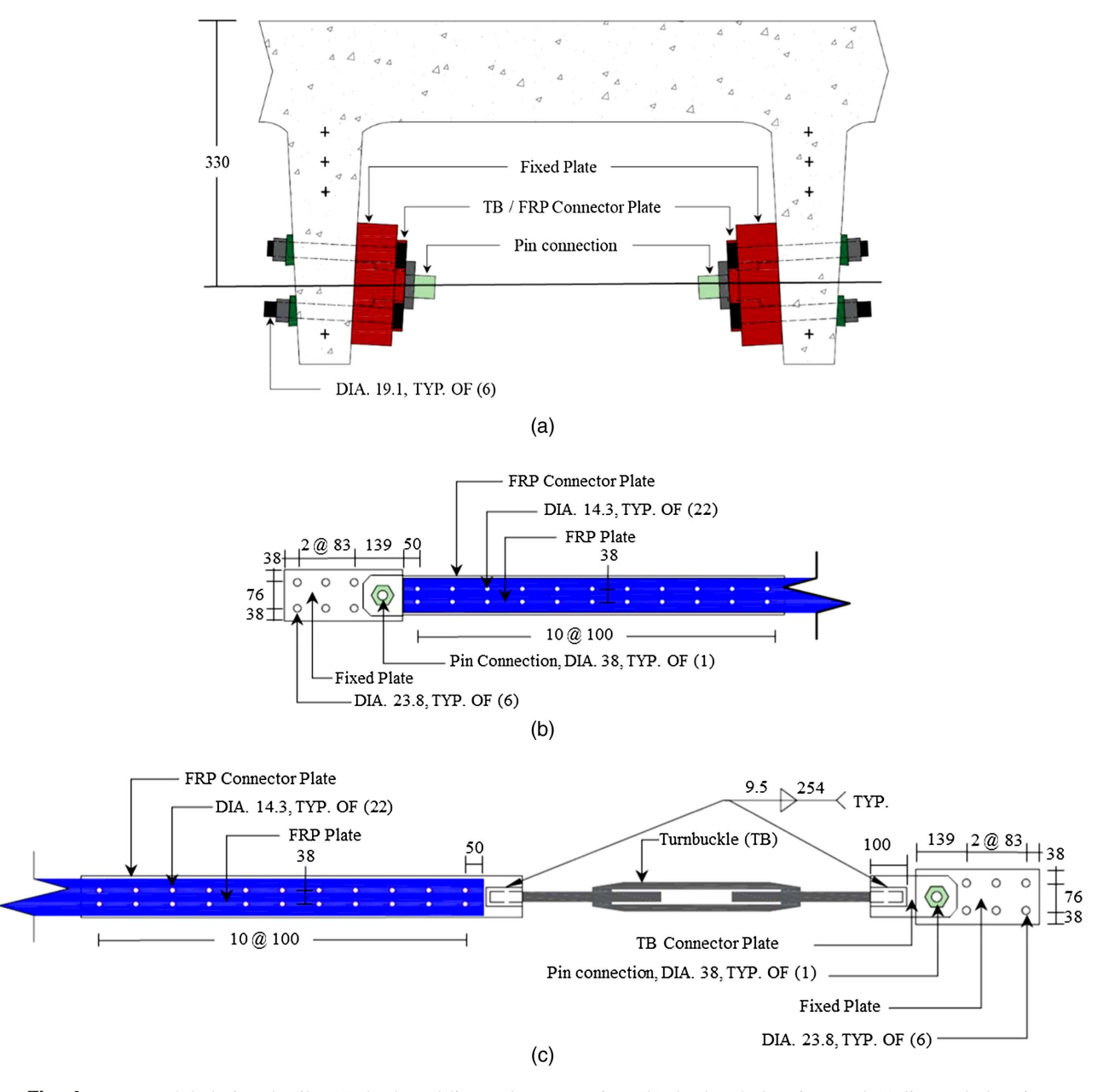
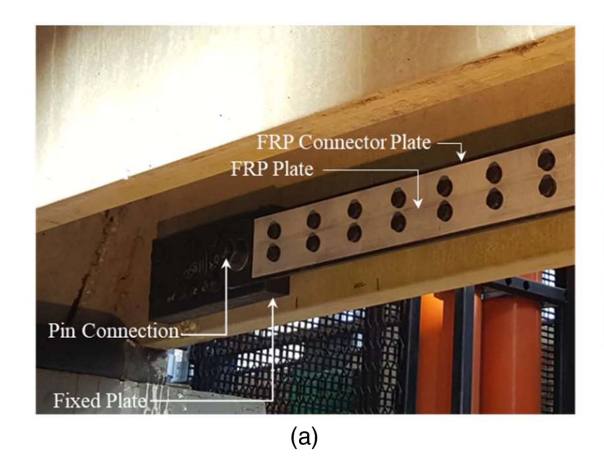


Fig. 4. MF-FRP 2.0 design details: (a) dead- and live-end cross-section; (b) dead-end elevation; and (c) live-end elevation.



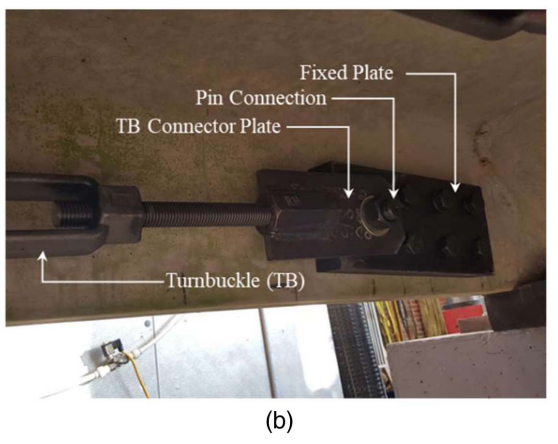


Fig. 5. MF-FRP 2.0 connection photos: (a) dead-end; and (b) live-end.

Concrete Splitting

Design guides that model concrete splitting behavior due to mechanical fasteners can be used to check the capacity of the concrete at each bolt. Eq. (2) is a model presented by Oehlers and Bradford (1995) that determines the minimum concrete splitting force for shear studs and bolted connections in composite steel and concrete elements, for which the length of the fastener is greater than $1.8d_{bolt}$:

$$P_{split} \approx 7\pi c d_{bolt} f_t \left(1 - \frac{d_{bolt}}{2c} \right)^{-2} \tag{2}$$

where P_{split} = minimum force at which splitting occurs; d_{bolt} = diameter of the bolt; c = concrete cover to the side of the bolt; and f_t = splitting tensile strength of the concrete in the strengthened member. Using 12.7-mm (0.5-in.) diameter bolts, a minimum concrete cover of 19 mm (0.75 in.), and concrete splitting tensile strength of 2.92 MPa (425 psi), P_{split} for a typical C-channel section with the retroit installed is 35.1 kN (7.9 kips) per bolt at the dead-end of MF-FRP 1.0. Assuming a uniform distribution of force in the FRP plate at ultimate load conditions, the maximum force per bolt is 10.2 kN (2.3 kips), which is below the splitting force. Therefore, force transfer between the FRP plate and the concrete substrate at the dead-end of MF-FRP 1.0 will not result in concrete splitting.

Using Eq. (2) to check concrete splitting at the live-end of MF-FRP 1.0, the minimum P_{split} is 87.6 kN (19.7 kips) per bolt, and the maximum force per bolt—assuming uniform distribution at ultimate load conditions—is 33.4 kN (8.3 kips) per bolt. Therefore, the bearing force at the bolts on the live-end of MF-FRP 1.0 and both ends of MF-FRP 2.0 will not result in concrete splitting.

The 76.2-mm (3.0-in.) transverse spacing and 82.6-mm (3.25-in.) longitudinal spacing of bolts at the dead- and live-ends of MF-FRP 2.0 (Fig. 4) are designed using Eqs. (3) and (4)

$$s_L \ge 1.4b_{eff} \tag{3}$$

and

$$s_T \ge b_{eff} \tag{4}$$

where s_L = center-to-center longitudinal spacing of bolts; s_T = edge-to-edge transverse spacing of bolts; and b_{eff} = effective width of the connection. The calculated connection width was 57.2 mm (2.25 in.) (center-to-center spacing minus d_{bolt}) such that the minimum s_L was 80.0 mm (3.15 in.) and the minimum s_T was 57.2 mm

(2.25 in.) according to Eqs. (3) and (4). For convenience of design and installation, s_L was rounded up to 82.6 mm (3.25 in.).

Post-Tensioning

Restoration of prestress losses due to deterioration of the C-channel beam was achieved through post-tensioning of the FRP plate. The post-tensioning was delivered through the turnbuckle system at the live-end of the MF-FRP system [Figs. 2(d) and 4(c)]. To simulate field applications, the applied prestressing force in each FRP plate was determined through an application of Hooke's Law using Eqs. (5) and (6)

$$P_{FRP} = \frac{(\Delta L_p)(A_{FRP})(E_{FRP})}{L_a} \tag{5}$$

and

$$\Delta L_{TOT} = \Delta L_p + \Delta L_{slip} \tag{6}$$

where ΔL_p = change in length of the FRP plate due to the applied prestress force; L_g = gauge length over which ΔL_p is measured; A_{FRP} = cross-sectional area of the FRP; E_{FRP} = elastic modulus of the FRP; P_{FRP} = prestress force in the FRP; ΔL_{slip} = axial displacement of the FRP plate to account for bolt slip in the connections; and ΔL_{TOT} = total axial displacement required to achieve the desired P_{FRP} . For the FRP plate used in this study, A_{FRP} was 300 mm² (0.5 in.²), E_{FRP} was provided by the manufacturer as 62,190 MPa (9.02 × 10⁶ psi), and the design strength was 640 MPa (92,900 psi) (Strongwell 2016). During post-tensioning, the MF-FRP system remains within 41% of the 200 kN (45 kip) capacity of the MF-FRP connection and is well within the elastic limit. Therefore, Hooke's Law is an appropriate application at prestress load levels based on the linear behavior of the MF-FRP presented by McCoy et al. (2019).

Prior to post-tensioning, an indicator was affixed to the FRP, and a mark was placed on the interior of the stem near the live-end. A second mark was placed on the stem at the desired ΔL_{TOT} distance from the first mark (Fig. 6). The gauge length, L_g , was measured on each test specimen from the midpoint of the 22-bolt anchor zone at the dead-end to the indicator affixed to the FRP plate. The midpoint of the anchor zone was used because the elongation of the FRP plate through the 22-bolt anchor region was assumed to linearly decrease through the anchor region toward the end of the FRP plate. The measured L_g for each MF-FRP 1.0 specimen was 3,785 mm (149 in.), and the desired P_{FRP}

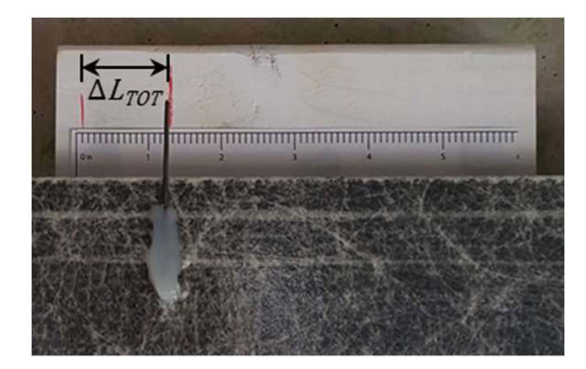


Fig. 6. ΔL_{TOT} measurement marks for MF-FRP 2.0 at $P_{FRP} = 82.3 \text{ kN}$ (18.5 kips).

was 82.3 kN (18.5 kips) to restore P_e for the HS strand that was cut to simulate moderate deterioration. Therefore, using Eq. 5, the desired ΔL_p was 15.5 mm (0.61 in.). The effect of a bolt slip between the FRP and steel plate, and the fixed plate and the concrete, was also included. $\Delta L_{\rm slip}$ was taken as the difference between the hole and bolt diameters. Therefore, ΔL_{slip} for MF-FRP 1.0 was 9.5 mm (0.375 in.). Using Eq. 6, ΔL_{TOT} for the MF-FRP 1.0 specimens was approximately 25 mm (1 in.). The measured L_g for the MF-FRP 2.0 specimens was 5,080 mm (200 in.), and the desired P_{FRP} remained 82.3 kN (18.5 kips). ΔL_{slip} for MF-FRP 2.0 was 10.3 mm (0.406 in.) and, using Eq. (5), ΔL_p was 24.3 mm (0.958 in.). Thus, ΔL_{TOT} for MF-FRP 2.0 was approximately 35 mm (1.38 in.). The marks for the ΔL_{TOT} measurement for MF-FRP 2.0 are provided in Fig. 6.

Throughout the post-tensioning process for all test specimens, FRP strain at midspan was monitored using electric resistance strain gauges. The strain gauge measurement was used to maintain consistency between test specimens and to confirm the application of Hooke's Law to determine P_{FRP} in the field in which strain gauges are not normally practical as a method for measuring the level of applied prestress force. Post-tensioning of the FRP was stopped when the measured strain in the FRP, ε_{FRP} , reached 4,100 $\mu\varepsilon$, the FRP strain which corresponds to $P_{FRP}=82.3$ kN (18.5 kips), at which point ΔL_{TOT} was confirmed with the marks on the FRP and concrete stem (Fig. 6).

MF-FRP 1.0 and MF-FRP 2.0 were installed on the side of the C-channel stem between the bottom prestressing strand and the three harped strands to deconflict the bolted connections and the prestressing strands (Figs. 2 and 4). Ideally, the MF-FRP retrofit solution would be installed on the bottom of the section, as is typical of flexural strengthening applications. However, the C-channel stem thickness at the bottom was 63.5 mm (2.5 in.), and the concrete cover for the bottom strand was 38 mm (1.5 in.) (Fig. 5). Therefore, it was determined that insufficient concrete cover existed to install the MF-FRP retrofit solution on the bottom of each stem.

Experimental Program

Six 9.14-m (30-ft) long C-channel beams were tested as part of this investigation. All C-channel beams were removed in relatively good condition from an existing structure. Two C-channel beams were tested without the MF-FRP retrofit installed—one undamaged (U) and one damaged (D)—to determine a control baseline prior to strengthening for each condition. Four C-channel beams were tested with the MF-FRP retrofit installed on the interior face of each stem, two undamaged (MF-FRP-U1 and MF-FRP-U2) and two

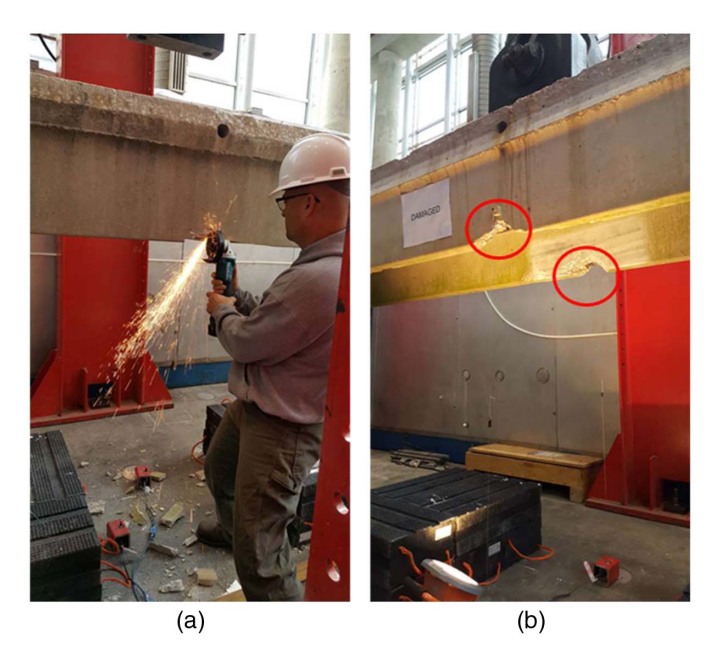


Fig. 7. Damaged C-channel beam: (a) cutting bottom strand; and (b) damage in both stems at midspan.

damaged (MF-FRP-D1 and MF-FRP-D2). Damage was induced in the lab by cutting the bottom prestressing strand in each stem at midspan (Fig. 7). The induced damage at midspan was used to simulate field deterioration with moderate prestress loss at the point of maximum internal moment in the C-channel beam loaded at the midspan.

Specimens MF-FRP-U1 and MF-FRP-D1 were tested with MF-FRP 1.0, and MF-FRP-U2 and MF-FRP-D2 were tested with MF-FRP 2.0. All MF-FRP specimens used one commercially available FRP plate per C-channel stem, indicated in Fig. 8, and discussed in detail in McCoy et al. (2019). Table 4 presents a summary of the test matrix for the six tested C-channel beams.

C-channel Beam Description

The six C-channel beams tested in this program were removed from North Carolina Bridge 380093, which carries State Route 1,156 (SR1156) across Owen Creek in Granville County, North Carolina. All beams selected for testing were interior undamaged girders in serviceable condition. These nominally identical beams allowed for controlling the damage of selected specimens to be implemented in the lab such that the results could be compared across all test specimens.

Fig. 9 provides the cross-section of the 9.14-m (30-ft) long C-channel beams. The beams were prestressed with 11.1-mm (7/16-in.) diameter HS, stress-relieved strands with an ultimate tension capacity of 1,860 MPa (270 ksi) (Table 5). The bottom HS strand in each stem was oriented parallel to the bottom of the stem; however, the three HS strands near the midheight of each stem were harped 90.4 mm (3.60 in.) at the midspan. Original design specifications required all strands to be stressed by the manufacturer with an initial prestressing force, P_i , of 96.5 kN (21.7 kips) (North Carolina DOT 1966). The C-channel beams were approximately 45 years old (400,000 + h) at the time of testing. Therefore, losses due to relaxation of the stress-relieved HS strands (not low-relaxation) can be estimated using the following (Nawy 2009):

$$\Delta f_{pR} = f'_{pi} \frac{\log t}{10} \left(\frac{f'_{pi}}{f_{py}} - 0.55 \right) \tag{7}$$

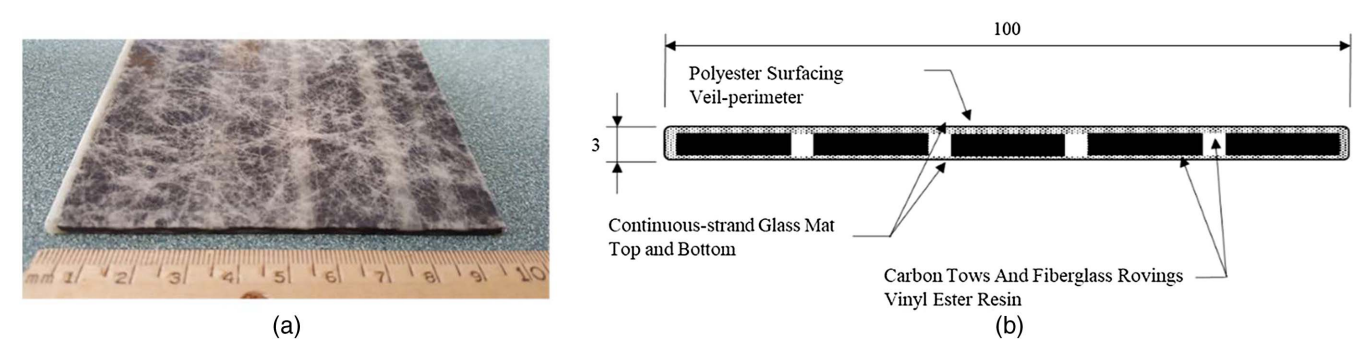


Fig. 8. FRP plate examined: (a) FRP plate sample; and (b) FRP cross-section. (Reprinted from McCoy et al. 2019, @ASCE.)

Table 4. C-channel test matrix

Specimen ID	Specimen description				
U	Undamaged control				
D	Damaged (deteriorated) control				
MF-FRP-U1	Undamaged with first version retrofit (MF-FRP 1.0)				
	installed on both stems				
MF-FRP-U2	Undamaged with improved retrofit (MF-FRP 2.0)				
	installed on both stems				
MF-FRP-D1	Damaged with MF-FRP 1.0 installed on both stems				
MF-FRP-D2	Damaged with MF-FRP 2.0 installed on both stems				

where Δf_{pR} = change in stress due to relaxation; t = time since initial applied prestress (hours); f'_{pi} = stress in the HS strand immediately after transfer—taken as 98% of f_{pi} to account for six hours of HS strand relaxation; and f_{py} = yield strength of the HS strand. Using Eq. (7), Δf_{pR} at the time of transfer, $\Delta f_{pR,transfer}$, is 27.5 MPa (4 ksi), assuming transfer occurs at six hours, and Δf_{pR} at 400,000 hours after transfer, $\Delta f_{pR,400k}$, is 153 MPa (22.2 ksi). Using the AASHTO (2017) lump sum approach, the predicted total prestress loss, Δf_{pT} , due to elastic shortening, shrinkage, and creep is 243 MPa (35.3 ksi). Hence, the effective prestress force at the time of testing, $P_{\text{eff},400k}$, was predicted to be 77.6 kN (17.4 kips), which is 80% of P_i and can be calculated using

$$P_{eff,400k} = (f'_{pi} - \Delta f_{pT})A_{ps} \tag{8}$$

Material properties (Table 5) and structural detailing information (Fig. 9) were extracted from structural drawings provided by the North Carolina DOT (1966).

Test Setup, Instrumentation, and Procedure

The test setup, indicated in Fig. 10, was modeled after a previous study that examined the behavior of similar C-channel beams strengthened with EB-FRP (Rosenboom and Rizkalla 2008). All C-channel beams were loaded in three-point bending with a 980 kN (220 kip) +/- 0.25% capacity load cell and hydraulic actuator mounted on a steel frame at the beam midspan. The load was applied with a 250×510 mm (10×20 in.) steel bearing plate in accordance with AASHTO (2017) bearing area requirements for wheel loading. Neoprene bearing pads on concrete blocks were used at the supports to simulate field conditions. The bearing width of each neoprene pad was 190 mm (7.5 in.), creating a span length of 8.95 m (29.4 ft) (Fig. 10). Prior to testing, all specimens were instrumented with string potentiometers at each quarter-span point and midspan point of the front stem, and at the midspan point of the rear stem. Additionally, two linear potentiometers were used to measure vertical displacement due to deformation of the neoprene bearing pads at the supports. Electric resistance strain gauges were attached to all FRP plates at midspan along the centroidal axis of the FRP plate to measure axial strain throughout the test.

All specimens were tested to failure under displacement-controlled conditions at a rate of 6.4 mm (0.25 in.) per minute from

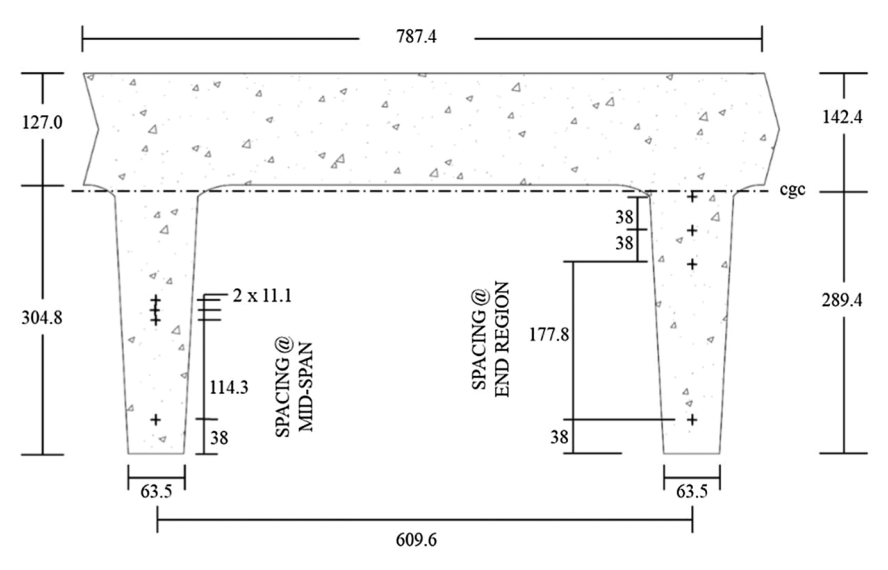


Fig. 9. C-channel cross-section details. (Data from NCDOT 1966.)

Table 5. C-channel specified material properties

Concrete details					
Detail parameter	Parameter value				
Design compressive strength, f'_c (MPa/psi)	35.5/5,000				
Compressive strength at transfer of prestress force,	27.6/4,000				
f_{ci} (MPa/psi)					
Compressive strength at time of testing, f_c (MPa/psi) ^a	68.9/10,000				
Cross-sectional area (mm ² /in. ²)	170,970/265				
Strong axis moment of inertia, I_{yy} (mm ⁴ /in. ⁴)	$119 \times 10^8 / 28,600$				
Prestressing strand details					
Ultimate strength, f_{pu} (MPa/ksi)	1,860/270				
Yield strength, f_{py} (MPa/ksi)	1,580/230				
Initial stress, f_{pi} (MPa/ksi)	1,300/189				
Transfer stress, f'_{ni} (MPa/ksi)	1,273/185				
Diameter (mm/in)	11.1/0.4375				
Area, A_{ps} (mm ² /in ²)	75.3/0.1167				
Ultimate prestress force, P_u (kN/kips) ^b	138/31.5				
Initial prestress force, P_i (kN/kips) ^c	96.5/21.7				
Effective prestress force at 400,000 h, $P_{eff,400k}$ (kN/kips) ^d	82.3/18.5				
Number of strands	8				

Source: Data from NCDOT (1966).

0 to 71.3 kN (0 to16.0 kips) of applied load, after which the rate was increased to 12.7 mm (0.5 in.) per minute through failure. The 71.3 kN (16.0 kips) applied load corresponds to an internal moment of 163 kN \cdot m (120 k \cdot ft) at midspan, which is the live load moment generated by the H-15 vehicle loading condition, including impact, along a single wheel line for a 9.1-m (30-ft) span length (AASHTO 2018). The H-15 is the original operating rating for the C-channel beams examined in this study (North Carolina

DOT 1966), and the H-15 live load moment assumes that no load transfer occurs between adjacent beams in accordance with the AASHTO (2018) load rating analysis guidelines.

Results and Discussion

Test Results

Table 6 provides a summary of test results, including ultimate load capacity and failure mode for all C-channel test specimens. Specimen U failed by concrete crushing (CC) at an applied load of 132 kN (29.6 kips). This ultimate capacity is 185% of the H-15 internal live load moment and serves as a benchmark for the MF-FRP-D1 and MF-FRP-D2 test specimens.

Specimen D also failed by concrete crushing at an applied load of 83.4 kN (18.7 kips). The induced damage to simulate moderate deterioration in the field resulted in a 37% reduction in capacity compared with Specimen U.

MF-FRP-U1 experienced an 18% increase in flexural capacity over U and failed by FRP longitudinal splitting (LS) and rupture (R), followed by concrete crushing. MF-FRP-D1 experienced a 47% increase in flexural capacity over D but failed to reach the full undamaged capacity, achieving 93% of the capacity of Specimen U. MF-FRP-D1 also failed by FRP longitudinal splitting and rupture followed by concrete crushing. Although the MF-FRP 1.0 retrofit system did not restore the full undamaged capacity of the C-channel beam, the system did increase the capacity of the damaged beam such that it exceeded the H-15 live load by approximately 52 kN (12 kips)—a factor of safety of 1.7; however, Specimen U failed at just 12 kN (3 kips) higher than the H-15 live load—a factor of safety of 1.2.

The midspan load-deflection behavior for all tests is provided in Fig. 11. Midspan deflection was determined by averaging the deflection at each stem measured by the two string potentiometers and subtracting the average vertical displacement at the supports

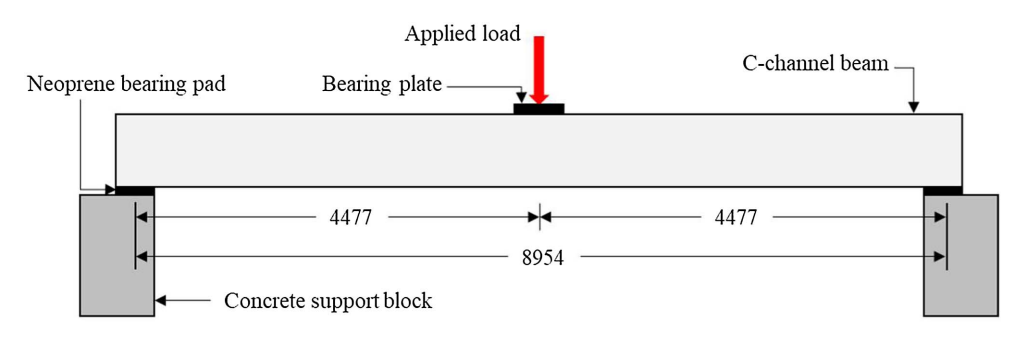


Fig. 10. Test setup.

Table 6. C-channel test results summary

Specimen ID	U	D	MF-FRP-U1	MF-FRP-U2	MF-FRP-D1	MF-FRP-D2
H-15 live load [kN (kips)]	71.3 (16.0)	71.3 (16.0)	71.3 (16.0)	71.3 (16.0)	71.3 (16.0)	71.3 (16.0)
Ultimate load [kN (kips)]	132 (29.6)	83.6 (18.8)	156 (35.1)	166 (37.3)	123 (27.6)	116 (26.1)
Percent increase from U (%)	_	-36.6	18.1	25.8	-6.85	-12.1
Percent capacity of H-15 (%)	185	117	219	233	172	163
Maximum measured FRP tensile strain ($\mu\varepsilon$)	_	_	7,380	6,425	7,980	6,712
Maximum FRP tensile force ^a [kN (kips)]	_	_	148 (33.2)	128 (29.0)	160 (36.0)	135 (30.3)
Failure mode	CC	CC	LS/R, CC	CC	LS/R, CC	CC

Note: LS = longitudinal splitting; R = rupture; and CC = concrete crushing.

^aCalculated from cores removed at time of testing.

^bCalculated with f_{pu} and A_{ps}.

^cCalculated with f_{pi} and A_{ps} .

^dCalculated with Eq. (8).

^aObtained from strain gauge and application of Hooke's law.

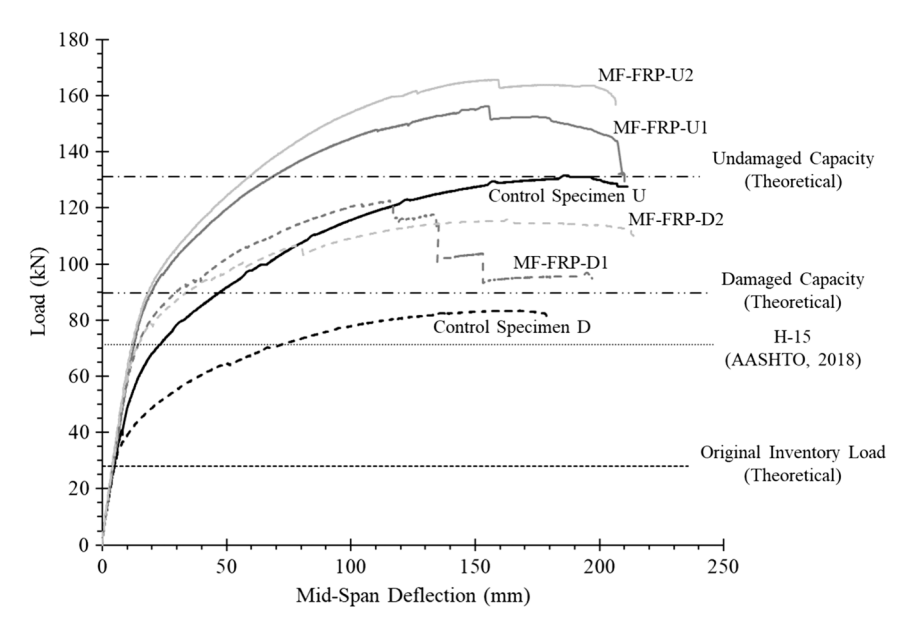


Fig. 11. Full-scale C-channel beam load-deflection results.

measured by the linear potentiometers. The progressive FRP longitudinal splitting and rupture failure of MF-FRP-D1 is visualized in the load-deflection curves (Fig. 11) with a "stepwise" decrease after ultimate load due to progressive loss in the FRP cross-sectional area. MF-FRP-U1 did not experience incremental FRP rupture but, rather, instantaneous longitudinal splitting and rupture failure just before concrete crushing, which is visualized as an instantaneous drop in load at approximately 200 mm (7.87 in.) of midspan deflection.

The load-deflection behavior in Fig. 11 is also compared with the theoretical inventory load, undamaged capacity, and damaged capacity. The theoretical inventory load is determined by calculating the internal moment at which the concrete tensile stress is 0 for an undamaged C-channel beam. Therefore, using the calculations presented by McCoy (2019), an internal live load moment, including impact, of 64.1 kN · m (47.3 k · ft) is considered the inventory load for a candidate bridge in a coastal region (the most conservative inventory load situation), which corresponds to an applied load of 28 kN (6.3 kips). This is provided in Fig. 11 and lies well within the elastic region of the load-deflection curves for all test specimens, which indicates that the beam would experience no damage from continued loading over an extended period at this inventory load. The calculations for the theoretical undamaged and damaged nominal maximum moment capacities are also presented in detail by McCoy (2019). The theoretical undamaged nominal moment capacity, $M_{n,undamaged}$, is 300 kN·m (221 k·ft), and the theoretical damaged nominal moment capacity, $M_{n,damaged}$, is 205 kN·m (151 k·ft), which corresponds to an applied load of 131 kN (29.5 kips) and 89.4 kN (20.1 kips), respectively (Fig. 11). The maximum applied load for Specimen U coincides very well with the theoretical undamaged capacity at 101% of $M_{n,undamaged}$, and the applied load for Specimen D is 94% of $M_{n,damaged}$ (see Table 6; Fig. 11).

The applied load that generates the H-15 live load moment, including impact, (AASHTO 2018) is also shown in Fig. 11. For Specimen U, the load-deflection curve intersects with the H-15 live load just beyond the elastic region at approximately 25 mm (1 in.) of midspan deflection. This indicates that incremental damage may occur at this load, which corresponds to the definition of the operating rating (AASHTO 2018). Although the maximum load for

MF-FRP-D1 is 93% of the maximum load for Specimen U, the load-deflection curve for MF-FRP-D1 intersects with the H-15 live load at approximately 10 mm (0.4 in.), which is less than 50% of the H-15 live load deflection for Specimen U and is within the elastic region of the strengthened damaged section. This indicates that the MF-FRP 1.0 system is capable of restoring the H-15 live load capacity of the beam despite the premature longitudinal splitting failure of the FRP. This led to the development of the MF-FRP 2.0 system described previously, which was designed to prevent the premature FRP failure, enabling the beam to fail by concrete crushing.

During the MF-FRP-U1 and MF-FRP-D1 tests, bending of the FRP plate about its strong axis at the dead-end was observed, as can be seen in Fig. 12(a). This was due to the fixed condition of the 22-bolt dead-end connection and the side-stem application of the FRP, resulting in the combination of flexural and axial tensile stresses in the FRP, causing longitudinal splitting failure of the FRP plate [Figs. 12(b and c)]. McCoy et al. (2019) determined that the capacity of the 22-bolt connection in uniaxial tension is 200 kN (45 kips); however, the FRP plates on MF-FRP-U1 and MF-FRP-D1 ruptured at 148 kN (33 kips) and 160 kN (36 kips), respectively, well below the expected capacity for the connection. The longitudinal splitting behavior resulted from the shear failure of the transverse glass fibers in the FRP plate and is discussed in detail in McCoy et al. (2019). To reduce this increased stress due to flexure in the FRP plate, the MF-FRP 2.0 connection design used a pin connection (Figs. 4 and 5) to allow rotation at each end of the C-channel such that the FRP plate remained in uniaxial tension throughout the loading of the C-channel, eliminating the development of flexural stresses in the FRP. This prevents longitudinal splitting rupture of the FRP and increases the efficiency of the MF-FRP system.

MF-FRP-U2 experienced a 26% increase in capacity compared with control Specimen U, and the ultimate load capacity for MF-FRP-D2 was 88% of the capacity for control Specimen U and 94% of the ultimate capacity of MF-FRP-D1. The reduction in the capacity of MF-FRP-D2 compared with MF-FRP-D1 was due to the greater reduction in the effective depth of the MF-FRP as the beam deflects under increasing applied load and the lack of moment developed in the FRP plate. The reduced effective depth of the MF-FRP is discussed subsequently. Although the capacity

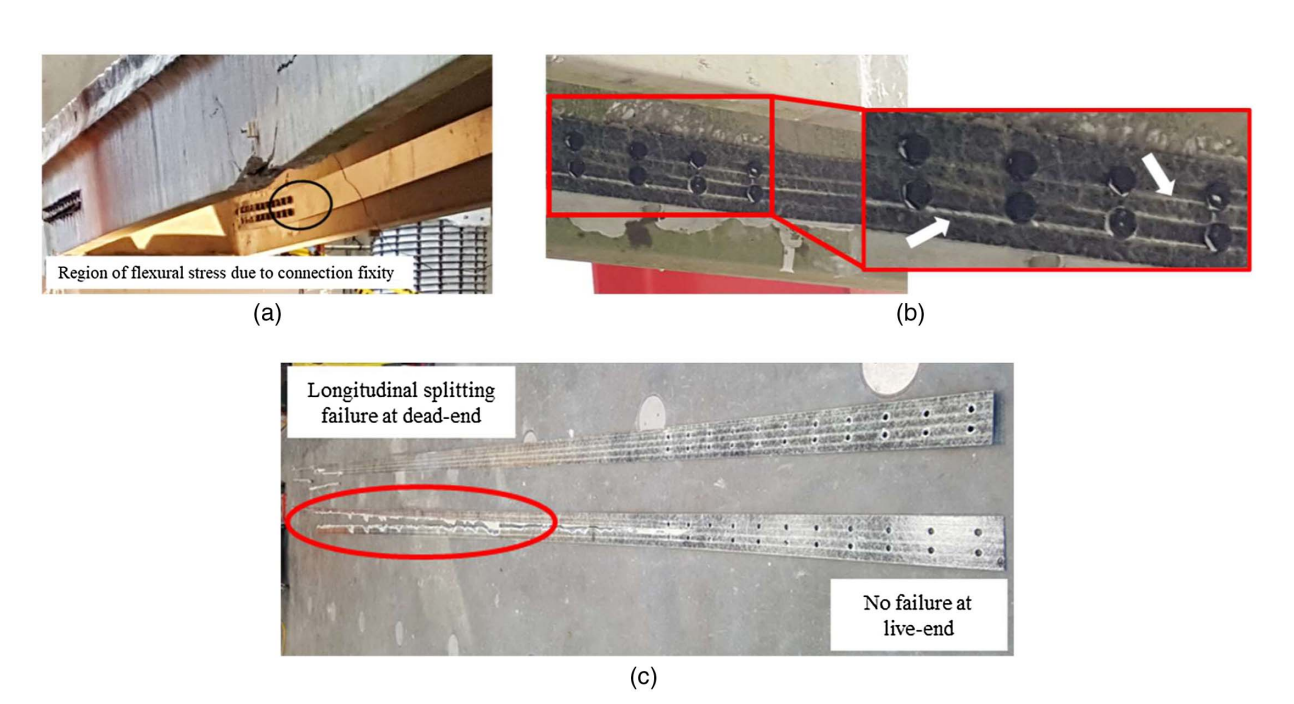


Fig. 12. FRP failure mode for MF-FRP 1.0: (a) flexural region; (b) longitudinal splitting due to flexure; and (c) failed FRP.

of MF-FRP-D2 was less than MF-FRP-D1, the MF-FRP 2.0 system increased the damaged stiffness and capacity of the C-channel such that the H-15 operating load was within the elastic region of the load-deflection curve; therefore, the MF-FRP 2.0 system restored both the inventory and operating ratings of the damaged C-channel to predamaged levels, enabling posted load restrictions and detours to be removed.

Both MF-FRP-U2 and MF-FRP-D2 failed by concrete crushing only. The FRP in MF-FRP-U2 and MF-FRP-D2 did not experience longitudinal splitting or rupture, as in MF-FRP-U1 and MF-FRP-D1. Consequently, a more ductile failure of MF-FRP-D2 was observed compared with that of MF-FRP-D1. This ductile failure of the MF-FRP 2.0 system design, visualized in the extended load plateau of MF-FRP-D2, is similar to that of Specimen U and is a more desirable failure than the brittle failure of MF-FRP-D1. Additionally, the FRP in MF-FRP 2.0 achieved a maximum tensile force of 128 kN (29.0 kips) and 135 kN (30.3 kips) for MF-FRP-U2 and MF-FRP-D2, respectively, leaving an FRP reserve capacity of approximately 67 kN (15 kips) for the MF-FRP 2.0 system, or 33% of the 200 kN (45 kips) capacity. This reserve capacity in the FRP allows for a higher prestress force to be applied if necessary, up to 98 kN (22 kips) based on the behavior presented by McCoy et al. (2019), to achieve restoration of inventory and operating ratings of the deteriorated C-channel.

The MF-FRP 1.0 and MF-FRP 2.0 systems experienced some minor local concrete splitting near the fixed plate connection. The local splitting occurred in line with the bottom prestressing strand in the stem and was due to the reduced concrete cover at the location of the prestressing strand. In all cases, the local splitting allowed for the prestressing strand to debond from the concrete but did not impact the overall performance of the MF-FRP retrofit solution. The debonding of the bottom prestressing strand is not of concern because the purpose of the MF-FRP retrofit solution is to restore the prestressing effects that would be lost due to deterioration in the field. In many field cases, the bottom prestressing strand is not present, and the concrete section is restored with a plain concrete patch (McCoy 2019).

Retrofit Installation

The 28 holes per stem required for the installation of MF-FRP 1.0 required extensive drilling in each concrete stem. The spalled concrete due to drilling at the dead-end required patchwork to provide a smooth surface to attach the FRP. The installation time for all field-level tasks (those tasks that must be completed at the bridge site in the field) was recorded to compare the installation efficiency of the two MF-FRP retrofit designs. The times presented in Table 7 indicate the time to install the MF-FRP retrofit system on both stems of a single C-channel and categorizes the total time for each task into working time, contributing time, and not working time. Working time (W) is time spent performing the actual task (i.e., drilling), contributing time (C) is time spent performing a supporting task (i.e., moving the dust collector during drilling), and not working time (NW) is all other time spent on the project (i.e., rest breaks).

For MF-FRP 1.0, holes were drilled from the exterior of the stem because the size of the hammer drill and length of the available bits prevented drilling from the interior. However, in a field installation, holes on interior beams would be drilled from the interior of the stem because adjacent beams would prevent access to the exterior of the stems with a hammer drill. However, access between beams is sufficient for the installation of washers and nuts on the exterior of the stem. Therefore, a compact hammer drill and bits were purchased for the installation of MF-FRP 2.0 such that holes could be drilled from the interior of the C-channel to replicate a field installation. Drilling holes from the interior of the stem also eliminated the need for grout at the dead-end, as previously mentioned. Therefore, grout installation at the dead-end is not included in the time analysis in Table 7.

The MF-FRP 2.0 design reduced the total number of field-level drilled holes per beam by more than 50% from 56 to 24, which reduced the time to drill the dead-end by 1.7 labor-hours (Table 7). With MF-FRP 2.0, the FRP plate was not attached directly to the stem, reducing the number of bolts placed in the field at the dead-end, which reduced the time to attach the live-end for MF-FRP 2.0 by 0.6 labor-hours. Additionally, the concrete drilling process for

Table 7. MF-FRP retrofit installation times for a single C-channel

	Installation time (labor-hours)							
	MF-FRP 1.0				MF-FRP 2.0			
Task	W	С	NW	Total	W	С	NW	Total
Locate steel	0.3	0.1	0	0.4	0.2	0.1	0	0.3
Drill live-end	0.8	0.5	0.8	2.0	0.5	0.5	0.3	1.3
Drill dead-end	1.0	1.0	1.0	3.0	0.5	0.5	0.3	1.3
Attach live-end	0.5	0.3	0.2	1.0	0.3	0.2	0	0.4
Attach dead-end	0.2	0.3	0	0.7	0.2	0.1	0	0.3
Post-tension FRP	0.4	0.5	0.4	1.2	0.3	0.3	0.0	0.7
Total	3.1	2.7	2.5	8.3	1.9	1.7	0.5	4.1
Percent of total (%)	37.7	32.7	29.6	100	46.9	40.8	12.2	100

the dead- and live-ends of MF-FRP 2.0 was optimized through the use of shop-prepared templates and drilling a 9.5-mm (0.125-in.) diameter pilot hole for each bolt, followed by incrementally increased diameters of 12.7 mm (0.5 in.), 19.1 mm (0.75 in.), and 22.2 mm (0.875 in.) to achieve the desired, over-sized hole diameter for the 19.1 mm (0.75 in.) diameter bolts. Incrementally increasing the hole diameter allowed for increased efficiency and a less labor-intensive drilling process, resulting in less break time (nonworking time). Further, incrementally increasing the diameter of each hole significantly reduced concrete spalling on the exterior of the stem, increasing the available concrete bearing surface concrete for each bolt. The reduction in installation time not only decreases labor costs but also limits muscle exertion and noise exposure, which leads to reduced worker fatigue, fewer errors, and fewer safety risks.

The time required for post-tensioning the FRP was the same for both MF-FRP 1.0 and MF-FRP 2.0. During post-tensioning, a large wrench was used to rotate the turnbuckle. A second wrench was used to hold the FRP connector plates to prevent them from rotating while the turnbuckle was tightened. To maintain the symmetry of internal forces on the C-channel stems, post-tensioning was applied in equal increments, alternating on each stem. If possible, it would also be appropriate to simultaneously post-tension the FRP plates.

An additional consideration with the MF-FRP 2.0 design was the weight of the individual components. The weight and total length of the live-end for MF-FRP 1.0—fixed plate, turnbuckle, and FRP connector plate [Fig. 2(d)]—was greater than 23.1 kg (51 lb), the maximum recommended weight limit (RWL) for a single-person, two-handed lift (NIOSH 1994) and, thus, required two people to lift the system into place during installation. However, MF-FRP 2.0 was designed such that the fixed plates could be installed individually, without the FRP connector plates or turnbuckle attached. After the fixed plate was installed, the FRP or turnbuckle connector plates could be hung from the connector pin. The total weight of the fixed plate was approximately 19.5 kg (43 lb), which is less than the RWL, allowing for a single-worker two-handed lift and increasing installation efficiency.

Shop-level tasks, such as cutting and drilling holes in the FRP plate and attaching the FRP plate to the FRP connector plates in MF-FRP 2.0, were not included in the installation time because they would be accomplished prior to crew mobilization. It is expected that DOT field maintenance personnel would take precut and predrilled FRP plates, preattached to steel FRP connector plates to the bridge site for installation. Therefore, only the tasks listed in Table 7 are necessary at the bridge site, minimizing field labor time and costs.

Fig. 13 provides a visual representation of the working, contributing, and not working times presented in Table 7. The complete

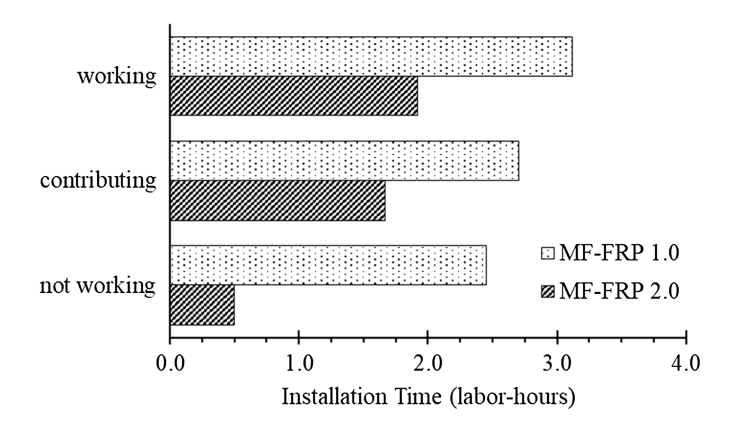


Fig. 13. Installation time comparison of MF-FRP 1.0 and MF-FRP 2.0 by time category.

process optimization for the installation of MF-FRP 2.0 reduced the total field-level installation time from 8.3 labor-hours for MF-FRP 1.0 to 4.1 labor-hours for MF-FRP 2.0 (Table 7)—a 53% reduction. The percentage of working time is increased from 38% of the total time for MF-FRP 1.0 to 47% of the total time for MF-FRP 2.0 (Table 7). Additionally, the percentage of not working time is reduced from 30% to 12% with the MF-FRP 2.0 design (Table 7). Important to note is that this installation time analysis was based on novice-level labor in a laboratory environment using two workers. Further optimization is likely with increased experience and number of workers. Therefore, it is recommended that field installation time analysis be included in future research planned for the installation of MF-FRP 2.0 on in-service candidate bridges with DOT maintenance personnel. It is also recommended that a fourworker crew size be employed in the field to allow the dead- and live-end activities to occur in parallel, providing greater optimization and a greater reduction in installation time.

Installation times presented are for a single C-channel beam. Deteriorated C-channel bridges often have between two and four deteriorated beams per span, with the greatest deterioration occurring on the exterior girders, as in the case study bridge presented by McCoy (2019). In candidate bridges with four deteriorated C-channel beams, the total installation time for MF-FRP 2.0 (excluding mobilization and demobilization of installation personnel) would be 16.4 labor-hours. A typical four-worker DOT maintenance crew has a total of 32 available labor-hours per eight-hour workday; therefore, it is feasible for a single span bridge with four deteriorated C-channel beams to be retrofitted with the MF-FRP 2.0 design in a single eight-hour workday, including mobilization and demobilization.

Table 8. C-channel concrete core data

			Strength	correction factor	, 2010)		
Specimen	Core	$f_{\rm core}$ [MPa (psi)]	$\overline{F_{\ell/d}}^{ m a}$	$F_{\rm dia}^{}$	F_{mc}^{c}	F_d^{d}	Adjusted f_{core} [MPa (psi)]
MF-FRP-D1	C1	73.4 (10,650)	0.95	1.0	0.96	1.06	74.0 (10,730)
	C2	84.4 (12,240)	0.94	1.0	0.96	1.06	84.3 (12,220)
	C3	72.0 (10,440)	0.94	1.0	0.96	1.06	71.4 (10,360)
	C4	84.2 (12,210)	0.95	1.0	0.96	1.06	84.3 (12,230)
MF-FRP-U2	C5	68.7 (9,960)	0.92	1.0	0.96	1.06	67.1 (9,730)
	C6	55.2 (8,000)	0.92	1.0	0.96	1.06	53.8 (7,810)
MF-FRP-D2	C7	62.0 (8,990)	0.92	1.0	0.96	1.06	60.3 (8,750)
	C8	78.5 (11,380)	0.92	1.0	0.96	1.06	77.6 (11,257)

^aLength-to-diameter ratio.

Concrete Strength

The specified concrete compressive strength, f_c' , of the C-channel beams examined in this study was 34.5 MPa (5,000 psi) (North Carolina DOT 1966). However, the equivalent in-place concrete compressive strength, $f'_{c,eq}$, of the beams at time of testing was desired to account for the actual concrete strength. After the completion of testing, cores were drilled from the flange of three of the six tested beams (MF-FRP-D1, MF-FRP-D2, and MF-FRP-U2) to determine $f'_{c,eq}$. A total of eight cores were drilled using a 100-mm (4-in.) outer diameter coring bit. The cores were drilled, prepared, and tested in accordance with ASTM C42 (ASTM 2018) and ACI 214.4 (ACI 2010). Individual core strengths, f_{core} , were adjusted to account for variability due to damage during drilling, moisture conditioning, and geometric properties of the core (Table 8). Adjusted core strengths were then considered the individual in-place strength of concrete, f_{ci} , at the location the core was extracted from in the C-channel beam [ACI 214.4 (ACI 2010)]. Using the ACI 214.4 Alternate Method (ACI 2010), $f'_{c,eq}$ is 56.6 MPa (8,210 psi) at the 90% confidence limit and is the recommended strength for use in the assessment of the existing beams. Differences between f'_c and $f'_{c,eq}$ are not uncommon in practice and are due to a number of factors, including concrete strength gain with maturity, concrete batch plant considerations, and high early concrete strength requirements during casting. Therefore, it is recommended that $f'_{c,eq}$ be determined as part of the assessment of all candidate bridges prior to the design and installation of the MF-FRP retrofit.

Predicted Flexural Capacity of Retrofitted C-Channel Beams

A layered-sectional analysis (LSA) approach (Collins and Mitchell 1997) was chosen to predict the flexural capacity of the C-channel beams presented in this paper. Appropriate constitutive models were selected for each of the materials in the nonlinear analysis to obtain reasonable predictions. Concrete in compression was modeled using the Jensen et al. (1998) relationship, whereas concrete in tension was taken to behave linearly until cracking. Concrete stress postcracking was taken as zero, and tension stiffening was not considered because flexural failure is assumed to occur at a cracked section in the analysis. The stress in the HS prestressing strands was modeled using the Mattock (1979) relationship based on the modified Ramberg-Osgood model (Ramberg and Osgood 1943). As previously discussed, the FRP stress follows Hooke's Law. A strain-based iterative procedure was conducted, ensuring equilibrium of axial forces and assuming that full strain

compatibility and plane sections remain plane to obtain the flexural capacity corresponding to the converged strain distribution. However, the post-tensioned MF-FRP was not bonded to the concrete substrate; therefore, the full strain compatibility assumption is inappropriate. This is similar to the behavior of external unbonded post-tensioned strands. Naaman and Alkhairi (1992) indicated that the strain of unbonded strands depends on the deformation of the member and can be taken as constant along the length of the strands. Harajli et al. (1999) observed that second-order effects need to be considered in the analysis of externally prestressed structures, in which the change in the eccentricity of the external unbonded prestress force is related to the member deflection. These factors are considered in the following flexural capacity analysis of the MF-FRP 2.0 retrofitted C-channel beams.

Fig. 14(a) indicates the discretized beam cross-section at midspan considering the second-order effects throughout testing; the global position of the MF-FRP remains constant, and the C-channel beam deflects with applied load, thereby reducing the effective depth of the centroid of the MF-FRP with increasing applied load. The effective depth of the centroid of the MF-FRP relative to the top compression surface of the C-channel beam before testing, $d_{FRP,i}$, and at failure, $d_{FRP,f}$, are provided in Fig. 14. The ultimate predictions are compared with the experimental results to validate the LSA approach.

To demonstrate the application and accuracy of the flexural capacity prediction, some experimental results were used in the analysis. In addition to material properties, the measured initial camber and the beam deflection to quantify $d_{FRP,f}$ and the MF-FRP strain, ε_{FRP} , corresponding to the maximum applied load were adopted in the analysis. The values used are provided in Table 9. The strain distribution is controlled by concrete crushing at $\varepsilon_{c,comp} = 0.003$, which is consistent with the experimentally observed failure mode. With these conditions, the strain distribution in the concrete section corresponding to the failure condition may be found by iteration based on achieving equilibrium of the axial forces.

Table 10 presents a comparison between the predicted flexural capacity and the experimental results for the unstrengthened control specimens (U and D) and the specimens retrofitted with MF-FRP 2.0 (MF-FRP-U2 and -D2). For the analysis of the unstrengthened control specimens, $\varepsilon_{FRP}=0$ in Fig. 14. For the analysis of the damaged specimens (D and MF-FRP-D2), $\varepsilon_{ps1}=0$ in Fig. 14 as the bottom HS strand was cut at the maximum moment location. Specimens MF-FRP-U1 and -D1 are not included in the comparison due to their premature failure of the FRP that was previously

^bCore diameter.

^cMoisture content.

^dDamage during coring.

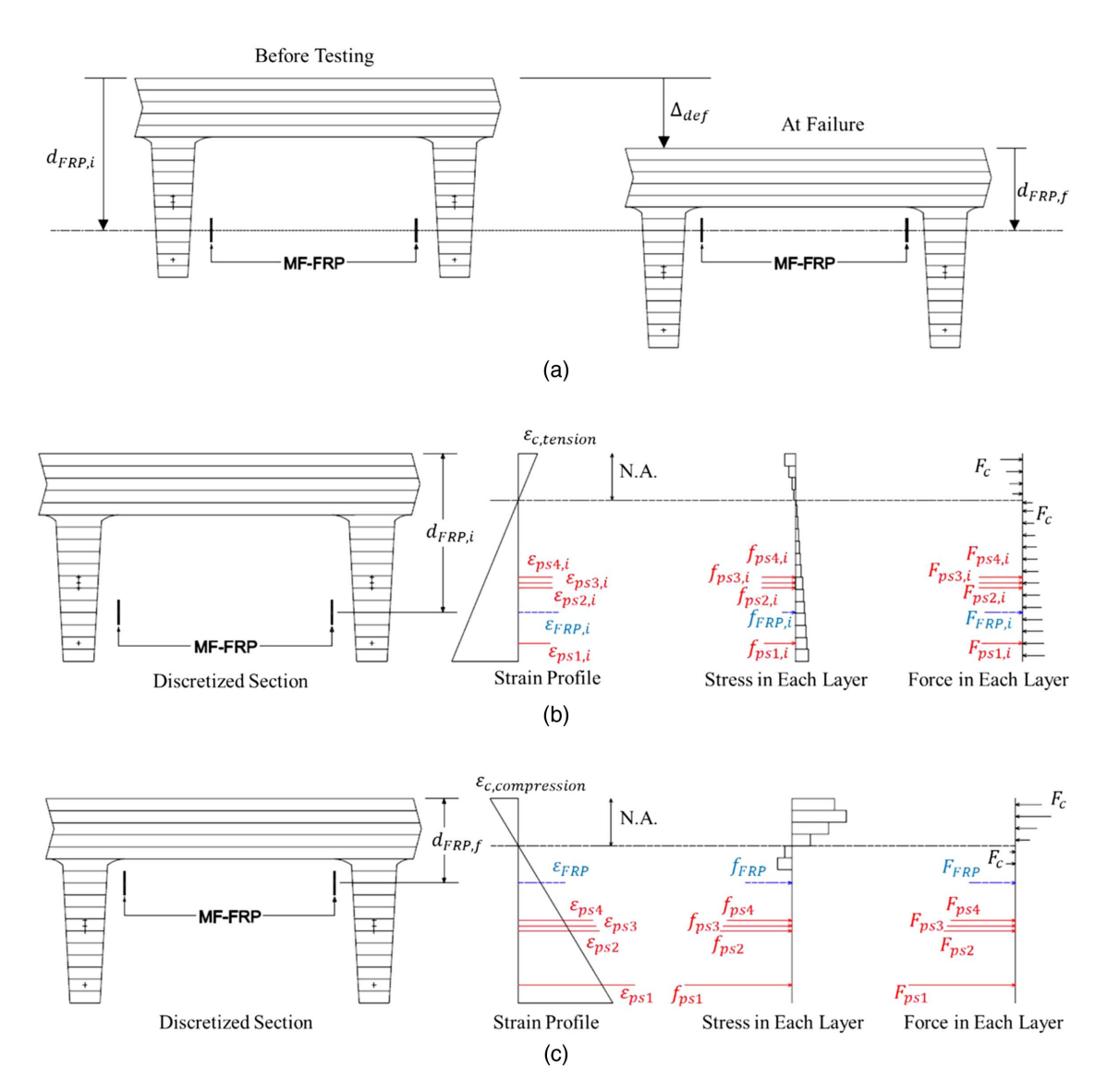


Fig. 14. Application of LSA: (a) global position of MF-FRP at midspan; (b) before testing; and (c) at failure.

Table 9. Experimental data used in LSA

Specimen ID	MF-FRP-U2	MF-FRP-D2
Initial camber [mm (in.)]	41.1 (1.62)	37.1 (1.46)
Deflection at maximum force,	171.5 (6.75)	174.0 (6.85)
$d_{FPR,f}$ [mm (in.)]		
Average FRP strain at maximum	5,597	6,146
force $(\mu \varepsilon)$		

discussed. Table 10 indicates that the LSA predictions for the retrofitted C-channels are within 5% of the experimental data. The LSA predictions for specimens U and D are within 8% and 14%,

respectively. This somewhat decreased accuracy of the LSA prediction may, in part, be due to a lack of actual concrete strength data for specimens U and D because cores were not taken from these beam specimens.

The ability of the LSA approach to predict the flexural behavior and capacity of retrofitted C-channel beams is demonstrated in this example. Future work involves adapting the analysis to predict the full moment-curvature response at any section along the length of the beam, which will enable the prediction of the full load-displacement response. This will require the development of models to predict the second-order effects—a function of the changing effective depth of the MF-FRP—and the MF-FRP strain at any given load for the unbonded post-tensioned system.

Table 10. Comparison of experimental and predicted results

Specimen ID	U	D	MF-FRP-U2	MF-FRP-D2
Experimental moment ^a $[kN \cdot m (kips \cdot ft)]$	295.4 (217.6)	187.1 (138.2)	371.4 (274.2)	259.6 (191.8)
Predicted moment $[kN \cdot m (kips \cdot ft)]$	319.0 (235.3)	217.7 (160.6)	353.2 (260.5)	256.5 (189.2)
Experimental/predicted	0.92	0.86	1.05	1.01

^aObtained from three-point bending load condition.

Conclusions and Recommendations

This research presents unique results related to the restoration of deteriorated prestressed concrete C-channel beams retrofitted with two designs for a post-tensioned MF-FRP retrofit solution. The test results and retrofitted C-channel behavior are compared with damaged (deteriorated) and undamaged control C-channel beams. The research presents the following conclusions:

- 1. MF-FRP 1.0 and MF-FRP 2.0 retrofit designs sufficiently restore a damaged C-channel with moderate deterioration at the maximum moment location such that the retrofitted C-channel is capable of supporting the original operating and inventory ratings. However, MF-FRP 1.0 allows an in-plane moment in the FRP plate to develop near the dead-end anchor zone, which introduces flexural stresses not present in uniaxial tension loading and should be avoided. This in-plane moment causes longitudinal splitting and rupture of the FRP plate at 69% of the uniaxial tension capacity.
- 2. MF-FRP 2.0 retrofit design resulted in failure by concrete crushing and a more ductile behavior compared with that of MF-FRP 1.0. The residual capacity of the FRP plate at concrete crushing is 33% of the FRP tensile capacity. This residual capacity in the FRP plate gives engineers the flexibility to increase the prestress force beyond the 82.3 kN (18.5 kips) applied in this investigation, up to 98 kN (22 kips). This would further increase the inventory and operating ratings of retrofitted C-channel beams.
- 3. MF-FRP 1.0 has a total installation time of 8.3 labor-hours for a single C-channel beam and 30% nonworking time. MF-FRP 2.0 reduces the total installation time to 4.1 labor-hours for a single C-channel beam, of which only 12% is nonworking time. The installation time for MF-FRP 2.0 is optimized such that a four-worker maintenance crew can install the retrofit on a typical deteriorated bridge within an eight-hour workday.
- 4. Both MF-FRP 1.0 and MF-FRP 2.0 require the concrete in the C-channel stems to be of sound quality at the location at which the retrofit is attached to the concrete substrate (fixed plates in MF-FRP 2.0). This should be verified through appropriate field inspection techniques [discussed in McCoy (2019)] prior to installation of the MF-FRP retrofit.
- The flexural capacity of an MF-FRP retrofitted C-channel beam can be predicted with very good accuracy using the LSA approach and actual material properties.

Worth noting is that the turnbuckle prestressing mechanism for both MF-FRP 1.0 and MF-FRP 2.0 remains in place, allowing for the prestress level in the system to be increased or decreased at a later time, if necessary. This also allows for the prestress in the retrofit to be increased or completely removed to either uninstall the MF-FRP retrofit system or replace the FRP plate, if necessary, to extend the life of the retrofit solution. Further, the connection hardware in the MF-FRP system can be reused in future applications, increasing the value of the system and any life-cycle cost analysis.

Additionally, all steel plate components for MF-FRP 1.0 and MF-FRP 2.0 were constructed of A572 Grade 50 steel, and A325 Grade 8 bolts were used for all bolted connections. For long-term durability in corrosive environments, such as bridges in coastal regions, it is recommended that connection components be constructed of stainless steel to resist corrosion and increase durability.

Current research is ongoing to examine the long-term performance of the retrofit solution under sustained and fatigue loading and to adapt the LSA approach to predict the full load-displacement response of retrofitted C-channel beams. Research to examine the

long-term behavior of the retrofit system on in-service C-channel bridges is also expected. Future research to demonstrate the application of the MF-FRP retrofit solution on a variety of prestressed concrete superstructure cross-sections, including hollow core slabs, is recommended.

Data Availability Statement

All of the data and models that support the findings of this study are available from the corresponding author on request.

Acknowledgments

The authors thank the North Carolina DOT and the NSF I/UCRC Center for the Integration of Composites into Infrastructure (CICI) for funding the research. Additionally, the authors acknowledge Cleveland City Forge for providing the turnbuckles used in MF-FRP 1.0 and MF-FRP 2.0 system designs, and Mr. William Briley at the North Carolina DOT Division 5 Bridge Maintenance Division for providing the C-channel beams for testing.

References

- AASHTO. 2017. *LRFD bridge design and specifications*. 8th ed. Washington, DC: AASHTO.
- AASHTO. 2018. The manual for bridge evaluation. 3rd ed., 674. Washington, DC: AASHTO.
- ACI (American Concrete Institute). 2010. *Guide for obtaining cores and interpreting compressive strength results*. ACI 214.4R. Farmington Hills, MI: ACI.
- AISC (American Institute of Steel Construction). 2015. *Steel construction manual*. 14th ed. Chicago, IL: AISC.
- Ammons, D. N. 2001. Municipal benchmarks: Assessing local performance and establishing community standards. 2nd ed. Thousand Oaks, CA: SAGE.
- ASTM. 2018. Standard test method for obtaining and testing drilled cores and sawed beams of concrete. ASTM C42. West Conshohocken, PA: ASTM.
- Bank, L. C., and D. Arora. 2007. "Analysis of RC beams strengthened with mechanically fastened FRP (MF-FRP) strips." *Compos. Struct.* 79 (2): 180–191. https://doi.org/10.1016/j.compstruct.2005.12.001.
- Bank, L. C., A. J. Lamanna, J. C. Ray, and G. I. Velazquez. 2002. Rapid strengthening of reinforced concrete beams with mechanically fastened, fiber-reinforced polymeric composite strips. Rep. No. ERDC/ GSL TR-02-4. Washington, DC: USACE.
- Borowicz, D. T. 2002. "Rapid strengthening of concrete beams with powder-actuated fastening systems and fiber reinforced polymer (FRP) composite materials." M.S. thesis, Dept. of Civil and Environmental Engineering, Univ. of Wisconsin-Madison.
- Cavalline, T., M. Whelan, B. Tempest, R. Goyal, and J. Ramsey. 2015. Determination of bridge deterioration models and bridge user costs for the NCDOT bridge management system. Technical Rep. No. FHWA/NC/2014-07. Raleigh, NC: North Carolina DOT.
- Collins, M. P., and D. Mitchell. 1997. Prestressed concrete structures, 766. Toronto: Response Publications.
- Dempsey, D., and D. W. Scott. 2006. "Wood members strengthened with mechanically fastened FRP strips." *J. Compos. Constr.* 10 (5): 392–398. https://doi.org/10.1061/(ASCE)1090-0268(2006)10:5(392).
- Ebead, U. 2011. "Hybrid externally bonded/mechanically fastened fiberreinforced polymer for RC beam strengthening." ACI Struct. J. 108 (6): 669–678.
- Ekenel, M., A. Rizzo, J. J. Myers, and A. Nanni. 2006. "Flexural fatigue behavior of reinforced concrete beams strengthened with FRP fabric and precured laminate systems." *J. Compos. Constr.* 10 (5): 433–442. https://doi.org/10.1061/(ASCE)1090-0268(2006)10:5(433).

- El-Maaddawy, T., A. Nessabi, and A. El-Dieb. 2013. "Flexural response of corroded reinforced concrete beams strengthened with powder-actuated fastened composites." J. Compos. Constr. 17 (6). https://doi.org/10 .1061/(ASCE)CC.1943-5614.0000395.
- El-Maaddawy, T. A. 2014. "Mechanically fastened composites for retrofitting corrosion-damaged reinforced-concrete beams: Experimental investigation." J. Compos. Constr. 18 (2). https://doi.org/10.1061 /(ASCE)CC.1943-5614.0000447.
- Elsayed, W. E., U. A. Ebead, and K. W. Neale. 2009. "Studies on mechanically fastened fiber-reinforced polymer strengthening systems." ACI Struct. J. 106 (1): 49–59.
- FEMA. 2017. Emergency vehicle size and weight guide. Technical Committee Rep. No. TC009-1. Washington, DC: FEMA.
- Galati, D., A. Rizzo, and F. Micelli. 2007. "Comparison of reinforced concrete beams strengthened with FRP precured laminate systems and tested under flexural loading." In *Proc.*, FRPRCS-8, 1618. Patras, Greece: Univ. of Patras.
- Harajli, M. H., N. Khairallah, and H. Nassif. 1999. "Externally prestressed members: Evaluation of second-order effects." J. Struct. Eng. 125 (10): 1151–1161. https://doi.org/10.1061/(ASCE)0733-9445(1999)125:10 (1151).
- Jensen, J., E. Thorenfeldt, and A. Tomaszewicz. 1988. "Structural properties of high-strength concrete and applications in design." In Vol. 3 of Proc., Int. Conf. on Behavior of Offshore Structures, 1129–1144. Trondheim, Norway: Tapir Publishers.
- Knight, D., P. Visintin, D. J. Oehlers, and M. S. Mohammed Ali. 2014. "Simulation of RC beams with mechanically fastened FRP strips." Compos. Struct. 114 (Aug): 99–106. https://doi.org/10.1016/j.compstruct.2014.04.012.
- Lamanna, A. J. 2002. "Flexural strengthening of reinforced concrete beams with mechanically fastened fiber reinforced polymer strips." Ph.D. dissertation, Dept. of Civil and Environmental Engineering, Univ. of Wisconsin-Madison.
- Lamanna, A. J., L. C. Bank, and D. W. Scott. 2001. "Flexural strengthening of RC beams using fasteners and FRP strips." ACI Struct. J. 98 (3): 368–376.
- Lamanna, A. J., L. C. Bank, and D. W. Scott. 2004. "Flexural strengthening of reinforced concrete beams by mechanically attaching fiberreinforced polymer strips." *J. Compos. Constr.* 8 (3): 203–210. https://doi.org/10.1061/(ASCE)1090-0268(2004)8:3(203).
- Lee, J. H., M. M. Lopez, and C. E. Bakis. 2009. "Slip effects in reinforced concrete beams with mechanically fastened FRP strip." Cem. Concr. Compos. 31 (7): 496–504. https://doi.org/10.1016/j.cemconcomp .2009.04.008.
- Loring, H. B., and W. G. Davids. 2015. "Mechanically fastened hybrid composite strips for flexural strengthening of concrete beams." *Constr. Build. Mater.* 76 (Feb): 118–129. https://doi.org/10.1016/j.conbuildmat.2014.11.059.
- Martin, J. A., and A. J. Lamanna. 2008. "Performance of mechanically fastened FRP strengthened concrete beams in flexure." *J. Compos. Constr.* 12 (3): 257–265. https://doi.org/10.1061/(ASCE)1090-0268(2008) 12:3(257).

- Mattock, A. H. 1979. "Flexural strength of prestressed concrete sections by programmable calculator." *PCI J.* 24 (1): 32–54. https://doi.org/10.15554/pcij.01011979.32.54.
- McCoy, B. C. 2019. "Design and implementation of a new retrofit for prestressed concrete bridge elements using mechanically fastened-fiber reinforced polymer." Ph.D. thesis, Dept. of Civil, Construction, and Environmental Engineering, North Carolina State Univ.
- McCoy, B. C., Z. Bourara, R. Seracino, and G. W. Lucier. 2019. Anchor bolt patterns for mechanically-fastened FRP plates. Reston, VA: ASCE. https://doi.org/10.1061/(ASCE)CC.1943-5614.0000951.
- Naaman, A. E., and F. M. Alkhairi. 1992. "Stress at ultimate in unbonded post-tensioning tendons. Part 2: Proposed methodology." ACI Struct. J. 88 (6): 683–692.
- Napoli, A., L. C. Bank, V. L. Brown, E. Martinelli, F. Matta, and R. Realfonzo. 2013. "Analysis and design of RC structures strengthened with mechanically fastened FRP laminates: A review." *Composites, Part B* 55: 386–399. https://doi.org/10.1016/j.compositesb.2013.06.038.
- Nawy, E. G. 2009. *Prestressed concrete: A fundamental approach*. 5th ed., 949. Boston: Prentice Hall.
- NIOSH (National Institute for Occupational Safety and Health). 1994. Applications manual for the revised NIOSH lifting equation. Cincinnati, OH: US Dept. of Health and Human Services, NIOSH.
- North Carolina DOT. 1966. Standard prestressed concrete channels 20 ft.-, 25 ft.-, and 30 ft.-Spans, 24 ft.-, 29 ft.-, and 34 ft.-roadways. Standard BMD-13. Raleigh, NC: North Carolina DOT.
- North Carolina DOT. 2018. "North Carolina statewide bridge inventory." Accessed December 12, 2018. https://www.ncdot.gov/initiatives-policies/Transportation/bridges/Documents/StatewideBridges.xls.
- Oehlers, D. J., and M. A. Bradford. 1995. *Composite steel and concrete structural members: Fundamental behavior*, 549. Kidlington, UK: Elsevier.
- OSHA (Department of Labor Occupational Safety and Health Administration). 2018. "Construction industry regulations." Accessed September 12, 2018. https://www.osha.gov/laws-regs/regulations/standardnumber/1926.
- Piatek, B., T. Siwowski, J. Michalowski, and S. Blazewicz. 2020. "Flexural strengthening of RC beams with prestressed CFRP strips: Development of novel anchor and tensioning system." *J. Compos. Constr.* 24 (3): 04020015. https://doi.org/10.1061/(ASCE)CC.1943-5614.0001020.
- Ramberg, W., and W. R. Osgood. 1943. Vol. 902 of Description of stressstrain curve by three parameters: NACA technical notes. Washington, DC: National Advisory Committee for Aeronautics.
- Realfonzo, R., E. Martinelli, A. Napoli, and B. Nunziata. 2013. "Experimental investigation of the mechanical connection between FRP laminates and concrete." *Composites, Part B* 45 (1): 341–355. https://doi.org/10.1016/j.compositesb.2012.05.010.
- Rosenboom, O., and S. H. Rizkalla. 2008. Experimental study of intermediate crack debonding in fiber-reinforced polymer strengthened beams, 41–50. Farmington Hills, MI: American Concrete Institute.
- Strongwell. 2016. "SAFSTRIP® fiber reinforced strengthening strip." Accessed November 13, 2017. https://www.strongwell.com.
- Tan, K. H., and R. A. Tjandra. 2007. "Strengthening of RC continuous beams by external prestressing." *J. Struct. Eng.* 133 (2): 195–204. https://doi.org/10.1061/(ASCE)0733-9445(2007)133:2(195).